Results in Chemistry 4 (2022) 100587

Contents lists available at ScienceDirect

Results in Chemistry

journal homepage: www.sciencedirect.com/journal/results-in-chemistry

The investigation of Mo_3Sb_7 and $Mo_3Sb_{7-x}Te_x$ as electrocatalysts for the hydrogen evolution reaction

James P. Fraser *, Alexey Y. Ganin *

School of Chemistry, University of Glasgow, Glasgow G12 8QQ, United Kingdom

ARTICLE INFO

Keywords:
Hydrogen
Water electrolysis
Electrocatalytic materials
Electrochemical measurements

ABSTRACT

Proton exchange membrane electrolysers are considered one of the most promising devices for storing the excess, intermittent energy generated by renewable sources through water electrolysis. Hydrogen production by electrolysis is currently facilitated by expensive noble metals that act as electrocatalysts. Therefore, the future development of the hydrogen evolution reaction (HER) relies on sourcing relatively inexpensive materials that can act as alternative catalysts to noble metals. Herein, we explore the catalytic activity of Mo_3Sb_7 towards the HER and the effect that tellurium doping has on the system. Mo_3Sb_7 showed a large overpotential of 570 mV at a current density of 10 mA cm^{-2}. However, the replacement of Sb with Te increased the stability of the catalyst and in the case of $Mo_3Sb_{5.4}Te_{1.6}$ reduced the overpotential required to achieve 10 mA cm^{-2} to 511 mV. This improvement in performance is also mirrored in the Tafel slopes of the materials with $Mo_3Sb_{5.4}Te_{1.6}$ having a Tafel slope of 136.2 ± 0.5 mV dec^{-1} compared to 167.5 ± 0.6 mV dec^{-1} exhibited by Mo_3Sb_7. Although the three compounds tested are suboptimal HER catalysts, compared to state-of-the-art materials, they nevertheless provide an interesting system to observe the effects of tellurium doping on the catalytic performance.

Introduction

Renewable energy sources will play a key role in the transition to a net zero emission economy, but one of the major challenges still associated with these intermittent sources is our ability to successfully manage the peaks and troughs in their supply and demand. In this regard, using excess electricity generated by solar or wind sources to split water into its constituent parts, hydrogen and oxygen, produces an excellent fuel in the form of hydrogen, allowing the excess energy to be stored for later use [1–3]. Of the technologies used for water splitting, it is proton exchange membrane (PEM) electrolysers that are considered the best option for integration with renewable energy sources. They benefit from being light-weight and compact and their rapid start-up and shut-down times are well suited to the intermittent nature of renewables [4]. A significant challenge facing PEM electrolysers is that they operate under acidic conditions. This necessitates the use of Pt group metals as catalysts as they can withstand the harsh operating conditions and are still the best performing materials available [5].

The costs and scarcity associated with the Pt group metals has driven a significant amount of research into finding earth-abundant, less expensive alternatives. Various types of materials have been studied in the search for suitable replacements for Pt group metals, including but not limited to; transition metal dichalcogenides (TMDs), ternary transition metal nitrides, traditional metal alloys and various nanostructured composite materials have been studied heavily in the hopes of finding a suitable replacement for Pt group metals [6–12]. In particular, the molybdenum based TMDs (MoS_2, $MoSe_2$, $MoTe_2$) have been studied heavily, owing to the favourable Gibbs free energy change of hydrogen adsorption that was calculated for MoS_2 [13–19]. $MoTe_2$ has advantages over the other two Mo TMDs, such as the stability of its metallic 1T'-phase, which can be synthesised directly, which is not the case for 1T-MoS_2 and 1T-$MoSe_2$. Metallic conductivity in an electrocatalyst is known to be beneficial to performance [20]. 1T'-$MoTe_2$ has also been shown to exhibit some intriguing electrochemical properties. For instance, McGlynn *et al* demonstrated that the catalytic activity of the material improved over time. They attributed this to the adsorption of hydrogen on specific Te sites, driving a lattice distortion in the $MoTe_2$ structure resulting in a more active catalyst [17]. This work illustrated that incorporation of Te into an electrocatalyst may be a promising way to boost performance.

One Mo based compound that has not currently been investigated for use as a HER catalyst is molybdenum antimonide, Mo_3Sb_7. This material

* Corresponding authors.
E-mail addresses: james.fraser@glasgow.ac.uk (J.P. Fraser), alexey.ganin@glasgow.ac.uk (A.Y. Ganin).

https://doi.org/10.1016/j.rechem.2022.100587
Received 25 July 2022; Accepted 16 October 2022
Available online 17 October 2022

has mainly been studied for its thermoelectric properties and potential application as an anode material for sodium- and lithium-ion batteries [21–24]. An interesting feature of this compound is the ability to replace up to 2 Sb atoms per formula unit with Te without changing the crystal structure of the parent compound. The $Mo_3Sb_{7-x}Te_x$ system therefore provides an interesting platform to study the influence of Te doping on catalytic activity without having to be concerned over structural changes. Mo_3Sb_7 is the only known compound in the Mo-Sb binary system and exhibits a body-centred cubic Ir_3Ge_7-type crystal structure [25]. The incorporation of Te into the structure is reported to result in a slight reduction in the length of the lattice parameter, *a*, as well as causing a transition from metallic to semiconducting behaviour [21,24].

In this work four different compounds of the $Mo_3Sb_{7-x}Te_x$ (x = 0, 1, 1.6, 2) series were synthesised *via* a solid-state procedure and studied using powder X-ray diffraction (PXRD) and Rietveld refinement. Three out of the four samples were confirmed to be phase pure, whilst an $MoTe_2$ impurity was found in $Mo_3Sb_5Te_2$. As such the three phase pure materials were studied using scanning electron microscopy (SEM) to ensure their morphologies were similar. The compounds were then tested electrochemically to determine their catalytic activity. Overall, the materials performed poorly, with large overpotentials and Mo_3Sb_7 exhibiting extremely poor stability. An interesting trend was observed with the addition of Te into the structure, with the stability of the materials increasing and an increase in catalytic performance observed for $Mo_3Sb_{5.4}Te_{1.6}$. This was evident in the lower overpotential of 511 mV required to reach the benchmark current density of 10 mA cm^{-2} compared to 570 mV for Mo_3Sb_7. This was also mirrored in the values of the Tafel slopes with a value of 136.2 ± 0.5 mV dec^{-1} obtained for $Mo_3Sb_{5.4}Te_{1.6}$ whilst Mo_3Sb_7 exhibited a Tafel slope of 167.5 ± 0.6 mV dec^{-1}.

Results and discussion

Synthesis and characterisation of Mo_3Sb_7 and $Mo_3Sb_{7-x}Te_x$

Mo_3Sb_7, Mo_3Sb_6Te, $Mo_3Sb_{5.4}Te_{1.6}$ and $Mo_3Sb_5Te_2$ were synthesised using a modified version of the solid-state procedure published by Dashjav *et al.* [21] Stoichiometric amounts of the elemental powders were mixed together, before being heated in evacuated quartz ampoules for several days (see Methods section for full details). Subsequently, the resulting grey powders were reground in a pestle and mortar before being measured by PXRD and studied using Rietveld refinement based on previously reported structural models for Mo_3Sb_7 and $Mo_3Sb_{5.4}Te_{1.6}$ [26,27].

The PXRD pattern of Mo_3Sb_7 is shown in Fig. S1. The results of the Rietveld refinement of the structural model (space group *Im*-3*m*) against the PXRD data is shown in Fig. S2. The experimental profile is consistent with the calculated one suggesting that the sample is a single-phase and free from impurities. Furthermore, the unit cell parameter obtained $a = 9.5651(1)$ Å is similar to the value of $a = 9.5692$ Å obtained by Okabe *et al.* [26].

Regarding the tellurium doped materials, both Mo_3Sb_6Te and $Mo_3Sb_{5.4}Te_{1.6}$ were synthesised as phase pure materials as evidenced by their PXRD patterns and subsequent Rietveld refinement (Figs. S3–S6).

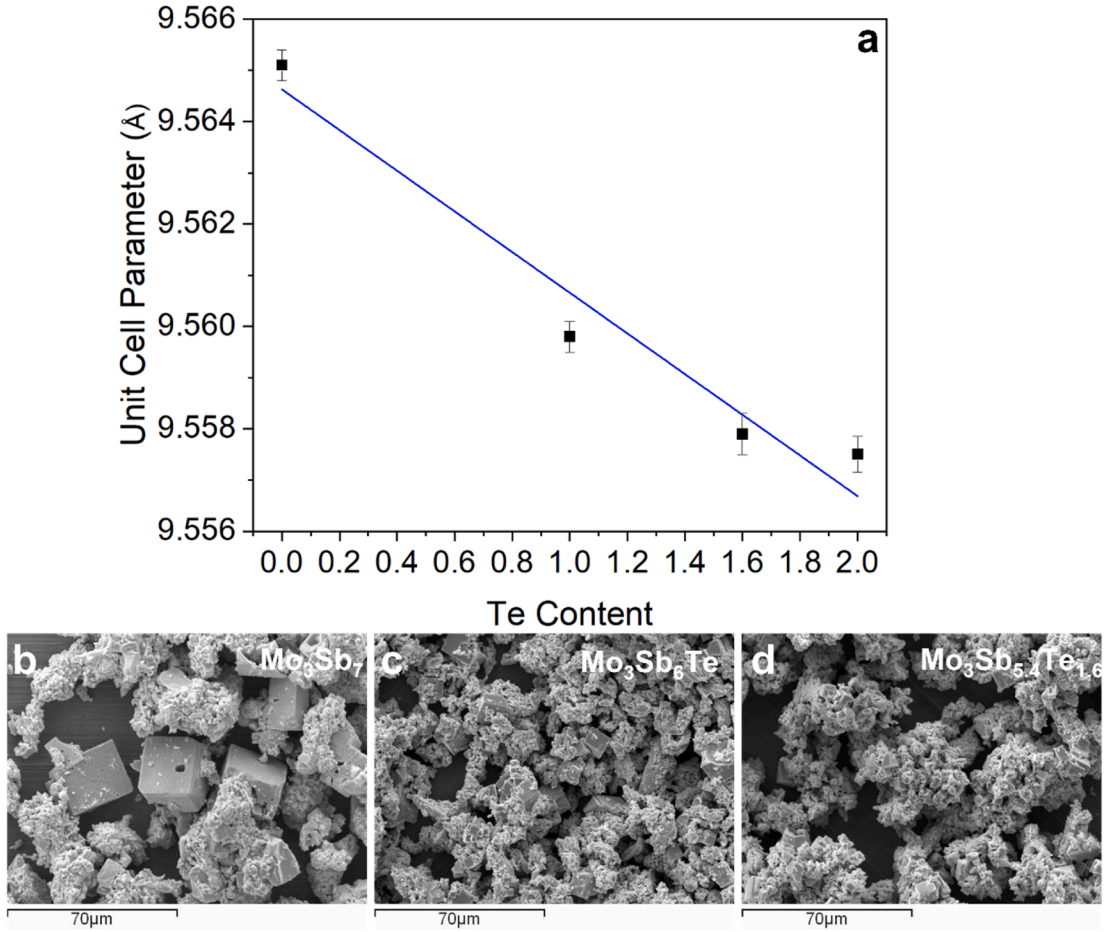

Fig. 1. A plot showing the relationship between the experimental unit cell parameter, *a*, and the Te doping level for $Mo_3Sb_{7-x}Te_x$ (x = 0, 1, 1.6, 2) (a). The blue solid line was obtained via a linear fit of the data. Also shown are SEM images of Mo_3Sb_7 (b), Mo_3Sb_6Te (c) and $Mo_3Sb_{5.4}Te_{1.6}$ (d). (For interpretation of the references to colour in this figure legend, the reader is referred to the web version of this article.)

However, in the case of $Mo_3Sb_5Te_2$ it is clear from the refinement performed (Figs. S5 & S6) that not all of the tellurium has entered the Mo_3Sb_7 structure, demonstrated by presence of 2H-$MoTe_2$ as an impurity. The formation of 2H-$MoTe_2$ as an impurity when trying to increase the Te content beyond 1.8 has also been observed in other works on the $Mo_3Sb_{7-x}Te_x$ system [24,28]. The unit cell parameters for the $Mo_3Sb_{7-x}Te_x$ materials decreases with increasing Te content compared to Mo_3Sb_7. For example, the *a* parameter for Mo_3Sb_6Te is 9.5598(1) Å whilst it is 9.5579 (6) Å for $Mo_3Sb_{5.4}Te_{1.6}$ and 9.5575 (3) Å for $Mo_3Sb_5Te_2$, respectively. A plot of the unit cell parameter versus tellurium content is shown in Fig. 1a. The decrease in the unit cell parameter, *a*, with increasing Te content can be understood by comparing the atomic radii of Sb and Te. Tellurium has a smaller atomic radius compared to antimony and therefore incorporation of it into the structure will lead to a decrease of the lattice parameter [24].

The morphology of an electrocatalyst can have a huge impact on its performance with nano-structuring a common technique used to improve catalytic performance by increasing the surface area, increasing the density of active sites or even improving electron transfer in the catalyst material [29]. Therefore, SEM was used to image Mo_3Sb_7, Mo_3Sb_6Te and $Mo_3Sb_{5.4}Te_{1.6}$ to ensure there were no major discrepancies in their morphologies. $Mo_3Sb_5Te_2$ was not examined *via* SEM due to the presence of the $MoTe_2$ impurity, meaning that the catalytic activity of the material could not be solely attributed to $Mo_3Sb_5Te_2$. 2H-$MoTe_2$ has previously been shown to be an active electrocatalyst for the hydrogen evolution reaction, albeit a poor one [30,31]. The three materials have broadly similar morphologies with cubic crystallites interspersed in more agglomerated material (Fig. 1b-d). The cubic microcrystals of Mo_3Sb_7 (Fig. 1b) appear significantly larger than those found in either of the Te doped materials (Fig. 1c & d) with an edge length of ~20 μm compared to 8–10 μm. Although the morphologies are similar; we could not exclude completely whether any the differences in catalytic performance were attributed to solely to the compositional variation in the three compounds.

Energy-dispersive X-ray spectroscopy (EDX) was used to determine the elemental composition of the $Mo_3Sb_{7-x}Te_x$ (x = 0, 1, 1.6) materials, with three spectra obtained from each sample and averaged to give the atomic percentages, which are summarised in Table 1.

It is evident from the EDX analysis that the compositions of Mo_3Sb_7 and Mo_3Sb_6Te are close to the ideal theoretical values within experimental error. However, there is a clear tellurium deficiency in the case of $Mo_3Sb_{5.4}Te_{1.6}$ with an atomic percentage of ~13 % compared to the theoretical value of 16 %. Nevertheless, there is still a sufficient variation in tellurium doping concentration to determine the impact this has on electrocatalytic performance.

Electrochemical behavior of Mo_3Sb_7 and $Mo_3Sb_{7-x}Te_x$

In order to test the electrocatalytic performance of the materials they were made into catalyst inks which were subsequently dropcast onto a glassy carbon working electrode. Cyclic voltammetry (CV) was then used to establish the overpotential required to achieve a current density of 10 mA cm^{-2}, which was taken as the figure of merit, for each material. In the case of Mo_3Sb_7, the material shows a veritable lack of stability, with the current densities achieved dropping rapidly with an increasing number of scans (Fig. 2a). For example, the overpotential required to achieve 10 mA cm^{-2} on the 2nd CV scan is −570 mV, but by the 20th scan this current density is not achievable. This poor performance is perhaps to be expected from Mo_3Sb_7 due to the inactivity of Sb-sites towards the hydrogen evolution reaction [32,33].

The addition of tellurium in the structure of Mo_3Sb_7 leads to a change in conductivity from metallic to semiconducting, which is typically not ideal for hydrogen evolution catalysts [20]. However, the activity of tellurium towards the HER has been previously reported and as such, replacing inactive Sb with Te may compensate for the change in electronic behaviour [34]. The CV scans obtained for Mo_3Sb_6Te (Fig. 2b) suggest that this level of Te doping is not sufficient to increase the catalytic performance with an overpotential of −595 mV required to reach the target current density on the 2nd cycle. Although, the stability of the material is much improved compared to Mo_3Sb_7, with an increase in overpotential of only 4 mV observed between the 2nd and 20th cycles. A further increase in the tellurium doping level does, however, lead to improved catalytic performance (Fig. 2c). The overpotential required by $Mo_3Sb_{5.4}Te_{1.6}$ to achieve the benchmark current density is −511 mV on the 2nd cycle and −514 mV after 20 cycles, respectively. Furthermore, the current densities reached by $Mo_3Sb_{5.4}Te_{1.6}$ are slightly higher than those achieved by Mo_3Sb_7, indicating that the level of Te doping in this case is sufficient to overcome the limitations of its semiconducting nature.

Tafel analysis was used to gain further insight into the catalytic activity of the $Mo_3Sb_{7-x}Te_x$ materials. The values obtained for the Tafel slopes (Fig. 2d) of the three materials mirrors their general catalytic performance. For example, Mo_3Sb_7 has the largest overpotential after 20 cycles and also the largest Tafel slope of 167.5 ± 0.6 mV dec^{-1}, which is higher than that of Mo_3Sb_6Te (153.6 ± 0.7 mV dec^{-1}) and $Mo_3Sb_{5.4}Te_{1.6}$ (136.2 ± 0.5 mV dec^{-1}). The values of the Tafel slopes obtained for these materials suggest that the kinetics of the HER are limited due to the inefficient adsorption of hydrogen on the catalyst surface [35].

In the wider context of state of the art HER catalysts these materials perform poorly compared to Pt, which only requires an overpotential of ~30 mV to reach 10 mA cm^{-2}, with a Tafel slope of around 30 mV $decade^{-1}$ [36]. However, when compared to TMD materials, $Mo_3Sb_{5.4}Te_{1.6}$ performs somewhat reasonably. Despite its semiconducting nature it outperforms two metallic TMDs in the form of 2H-TaS_2 and 1T'-WTe_2 and the semiconducting 2H-$MoTe_2$, which require overpotentials of 575, 692 and 650 mV to achieve 10 mA cm^{-2}, respectively [17,37,38].

However, other metallic TMDs such as 1T'-$MoTe_2$, 1T-MoS_2 and 2H-NbS_2 do outperform $Mo_3Sb_{5.4}Te_{1.6}$, with lower overpotentials and Tafel slopes [17,39]. A summary of the values obtained through the electrochemical testing of the $Mo_3Sb_{7-x}Te_x$ compounds and the values for the literature examples discussed above can be found in Table 2.

Conclusions

Four members of the $Mo_3Sb_{7-x}Te_x$ (x = 0, 1, 1.6, 2) family were synthesised *via* a simple solid-state procedure with the aim of testing their electrocatalytic activity towards the hydrogen evolution reaction. Through PXRD analysis and Rietveld refinement it was determined that Mo_3Sb_7, Mo_3Sb_6Te and $Mo_3Sb_{5.4}Te_{1.6}$ were synthesised as phase pure materials, whilst when x = 2 $MoTe_2$ was formed as an impurity, in line with other literature reports. SEM imaging revealed that the synthesis method resulted in the three phase pure materials having a similar morphology. Therefore, any discrepancies in catalytic activity could be

Table 1
EDX analysis showing the experimental atomic % composition of Mo_3Sb_7, Mo_3Sb_6Te and $Mo_3Sb_{5.4}Te_{1.6}$ compared to their theoretical values.

	Mo_3Sb_7 at. %		Mo_3Sb_6Te at. %			$Mo_3Sb_{5.4}Te_{1.6}$ at. %		
Element	Mo	Sb	Mo	Sb	Te	Mo	Sb	Te
Experimental	29.67 ± 1.02	71.33 ± 1.02	29.24 ± 1.07	59.88 ± 1.07	10.88 ± 1.07	29.87 ± 0.55	56.74 ± 0.55	13.39 ± 0.55
Theoretical	30	70	30	60	10	30	54	16

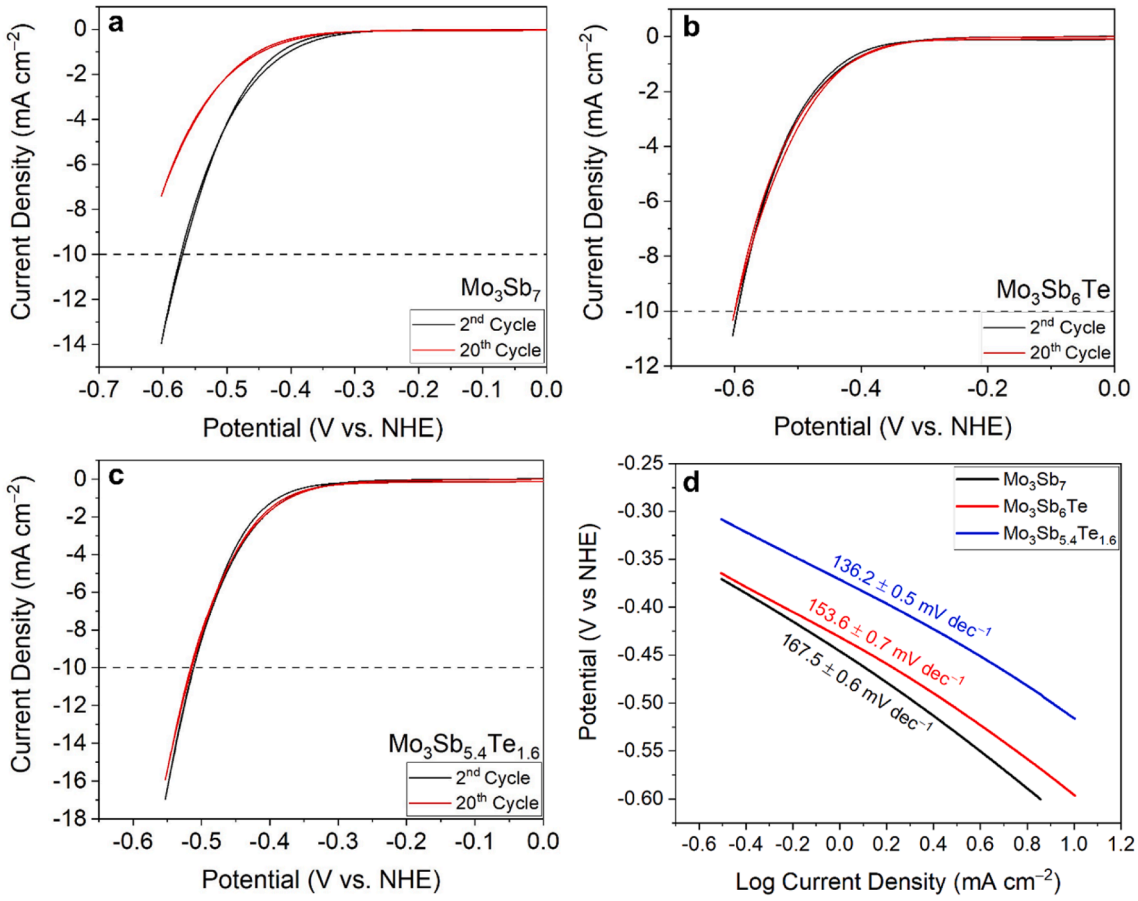

Fig. 2. Cyclic voltammograms obtained for the 2nd and 20th cycles of Mo_3Sb_7 (a), Mo_3Sb_6Te (b) and $Mo_3Sb_{5.4}Te_{1.6}$ (c). The benchmark current density of 10 mA cm^{-2} is highlighted with a dashed line. A plot of the Tafel slopes recorded for these compounds (d).

Table 2
A summary of the overpotentials for each material after 20 cycles and the value of their Tafel slopes and a comparison to literature values for Pt and several TMDs.

Material	η (mV) at 10 mA cm^{-2} (Cycled)	Tafel Slope (mv decade^{-1})	Reference
Mo_3Sb_7	n/a	167.5 ± 0.6	This work
Mo_3Sb_6Te	−599	153.6 ± 0.7	This work
$Mo_3Sb_{5.4}Te_{1.6}$	−514	136.2 ± 0.5	This work
Pt	−30	30	[36]
2H-$MoTe_2$	−650	159	[17]
1T'-$MoTe_2$	−340	78	[17]
1T-MoS_2	−250	50	[39]
2H-NbS_2	−290	140	[39]
2H-TaS_2	−575	>100	[37]
1T'-WTe_2	−692	169	[38]

attributed to compositional differences rather than a change in morphology or structure, as the incorporation of Te into Mo_3Sb_7 does not alter the cubic structure of the material. EDX spectra of the materials showed that the composition of Mo_3Sb_7 and Mo_3Sb_6Te matched the theoretical values, whilst $Mo_3Sb_{5.4}Te_{1.6}$ displayed a minor Te deficiency. There was still sufficient variation in the Te content of the compounds to determine the impact it had on their electrocatalytic ability, however.

The three phase pure materials were tested *via* cyclic voltammetry and Tafel analysis to establish their catalytic activity. Despite its metallic conductivity Mo_3Sb_7 performed poorly with a distinct lack of stability, evidenced by the drop off in the current densities reached between the 2nd and 20th cycle. The addition of Te into the structure improves the catalytic performance, with $Mo_3Sb_{5.4}Te_{1.6}$ requiring an overpotential of −511 mV to achieve a current density of 10 mA cm^{-2} compared to the −570 mV required by Mo_3Sb_7. The addition of Te also greatly improves the stability of the materials, with the overpotential of Mo_3Sb_6Te and $Mo_3Sb_{5.4}Te_{1.6}$ only increasing by 4 and 3 mV between the 2nd and 20th cycles, respectively.

Although the $Mo_3Sb_{7-x}Te_x$ materials were found to be poor HER catalysts when compared to Pt, $Mo_3Sb_{5.4}Te_{1.6}$ does outperform several TMDs including 2H-TaS_2, 1T'-WTe_2 and 2H-$MoTe_2$ in terms of overpotential and Tafel slope. This result highlights that as well as providing an interesting system to study the impact of tellurium doping on catalytic performance, $Mo_3Sb_{5.4}Te_{1.6}$ performs at a similar level to other earth-abundant materials that have been investigated as replacements for Pt group metals.

Methods

Mo_3Sb_7 and the $Mo_3Sb_{7-x}Te_x$ compounds were synthesised using a modified version of the literature procedure reported by Dashjav *et al.* [21] Elemental powders of molybdenum (Sigma Aldrich, 99.95 %), antimony (Alfa Aesar, 99.999 %) and tellurium (Alfa Aesar, 99.999 %) were ground together in the correct stoichiometric ratios in a pestle and mortar. The powders were sealed in quartz ampoules under a vacuum pressure of 1 × 10^{-3} mbar. Mo_3Sb_7 was heated in a Lenton furnace to 700 °C with a heating rate of 5 °C min^{-1} for 100 h before cooling to room temperature naturally, whilst $Mo_3Sb_{7-x}Te_x$ compounds were heated to 750 °C with a heating rate of 5 °C min^{-1} for 100 h before cooling to room temperature naturally.

PXRD measurements were performed on a PANalytical X'pert Pro diffractometer with a monochromatic Cu Kα (λ = 1.54178 Å) source operating in Bragg-Brentano geometry. Rietveld refinements were

carried out using GSAS-II software, with refined parameters including sample displacement, strain, crystallite broadening, atomic position and the unit cell parameters. In the Te-substituted samples, Te content was not refined, the unit cell parameter, *a*, was used to monitor Te doping, with a decrease in *a* observed for increasing Te content. The background was fitted using a Chebyshev polynomial whilst the peak shapes were described by a Pseudo-Voigt function.

Scanning Electron Microscopy (SEM) of Mo_3Sb_7 and $Mo_3Sb_{7-x}Te_x$ was performed on a Phillips XL30 ESEM instrument coupled with an Oxford Instruments X-act spectrometer for energy dispersive X-ray spectroscopy (EDX) measurements. The EDX was calibrated using INCA software with Cu as the calibration standard. To prepare samples for SEM/EDX around 1 mg of each compound was dispersed in 1 ml ethanol and sonicated for 10 min, before being dropcast onto copper foil and allowed to dry.

Electrochemical measurements of Mo_3Sb_7 and $Mo_3Sb_{7-x}Te_x$ compounds were performed using a glassy carbon working electrode (IJ Cambria) with a surface area of 0.071 cm^2.

The materials were prepared as catalyst inks and deposited onto the glassy carbon working electrode. This involved sonicating 10 mg of catalyst powder in 0.8 ml dimethylformamide with 80 μL of Nafion, which acts as a conductive binder to the substrate. 30 μL of the catalyst ink was then drop-cast on to a glassy carbon electrode with a surface area of 0.071 cm^2, before being allowed to dry for several hours, resulting in a catalyst loading of 5.3 mg cm^{-2}.

Cyclic voltammetry (CV) measurements were conducted with a Biologic SP-150 potentiostat utilising a single cell, three-electrode setup with 1 M H_2SO_4 as the electrolyte. Carbon felt (3.18 mm thick, 99.0 %, Alfa Aesar) was used as the counter electrode with a Ag/AgCl (Saturated NaCl, IJ Cambria) reference electrode whilst the glassy carbon electrode with deposited catalyst was used as the working electrode. A scan rate of 100 mV s^{-1} was used for the measurements and internal resistance was compensated for using the iR function of the potentiostat.

Electrode potentials were converted to the Normal Hydrogen Electrode (NHE) scale using the following equation:

$$E(NHE) = E(Ag/AgCl) + 0.197V$$

Declaration of Competing Interest

The authors declare that they have no known competing financial interests or personal relationships that could have appeared to influence the work reported in this paper.

Data availability

Data will be made available on request.

Appendix A. Supplementary data

Supplementary data to this article can be found online at https://doi.org/10.1016/j.rechem.2022.100587.

References

[1] I. Staffell, D. Scamman, A. Velazquez Abad, P. Balcombe, P.E. Dodds, P. Ekins, N. Shah, K.R. Ward, The role of hydrogen and fuel cells in the global energy system, Energy Environ. Sci. 12 (2) (2019) 463–491, https://doi.org/10.1039/C8EE01157E.

[2] S. Maddukuri, D. Malka, M.S. Chae, Y. Elias, S. Luski, D. Aurbach, On the challenge of large energy storage by electrochemical devices, Electrochim. Acta 354 (2020), 136771, https://doi.org/10.1016/j.electacta.2020.136771.

[3] A.I. Osman, N. Mehta, A.M. Elgarahy, M. Hefny, A. Al-Hinai, A.H. Al-Muhtaseb, D. W. Rooney, Hydrogen production, storage, utilisation and environmental impacts: a review, Environ. Chem. Lett. 20 (1) (2022) 153–188, https://doi.org/10.1007/s10311-021-01322-8.

[4] S. Shiva Kumar, V. Himabindu, Hydrogen production by PEM water electrolysis – a review, Mater. Sci. Energy Technol. 2 (3) (2019) 442–454, https://doi.org/10.1016/j.mset.2019.03.002.

[5] J.N. Hansen, H. Prats, K.K. Toudahl, N. Mørch Secher, K. Chan, J. Kibsgaard, I. Chorkendorff, Is there anything better than Pt for HER? ACS Energy Lett. 6 (4) (2021) 1175–1180, https://doi.org/10.1021/acsenergylett.1c00246.

[6] A.Y. Ganin, M.D. Symes, Towards the application of 2D metal dichalcogenides as hydrogen evolution electrocatalysts in proton exchange membrane electrolyzers, Curr. Opin. Electrochem. 34 (2022), 101001, https://doi.org/10.1016/j.coelec.2022.101001.

[7] I. Roger, M.A. Shipman, M.D. Symes, Earth-abundant catalysts for electrochemical and photoelectrochemical water splitting, Nat. Rev. Chem. 1 (1) (2017) 0003, https://doi.org/10.1038/s41570-016-0003.

[8] Y. Sun, L. Wang, O. Guselnikova, O. Semyonov, J. Fraser, Y. Zhou, N. López, A. Y. Ganin, Revealing the activity of Co3Mo3N and Co3Mo3N0.5 as electrocatalysts for the hydrogen evolution reaction, J. Mater. Chem. A Mater. 10 (2) (2022) 855–861, https://doi.org/10.1039/D1TA08389A.

[9] Y. Xu, R. Wang, J. Wang, J. Li, T. Jiao, Z. Liu, Facile fabrication of molybdenum compounds (Mo2C, MoP and MoS2) nanoclusters supported on N-doped reduced graphene oxide for highly efficient hydrogen evolution reaction over broad PH range, Chem. Eng. J. 417 (2021), 129233, https://doi.org/10.1016/j.cej.2021.129233.

[10] H. Deng, J. Yin, J. Ma, J. Zhou, L. Zhang, L. Gao, T. Jiao, Exploring the enhanced catalytic performance on nitro dyes via a novel template of flake-network Ni-Ti LDH/GO in-situ deposited with Ag3PO4 NPs, Appl. Surf. Sci. 543 (2021), 148821, https://doi.org/10.1016/j.apsusc.2020.148821.

[11] Y. Xu, R. Wang, J. Wang, Y. Zhang, T. Jiao, Encapsulation of Fe-CoP with P, N-Co-doped porous carbon matrix as a multifunctional catalyst for wide electrochemical applications, J. Energy Chem. 71 (2022) 36–44, https://doi.org/10.1016/j.jechem.2022.03.043.

[12] Y. Xu, R. Wang, Z. Liu, L. Gao, T. Jiao, Z. Liu, Ni2P/MoS2 interfacial structures loading on N-doped carbon matrix for highly efficient hydrogen evolution, Green Energy Environ. 7 (4) (2022) 829–839, https://doi.org/10.1016/j.gee.2020.12.008.

[13] J.K. Nørskov, T. Bligaard, A. Logadottir, J.R. Kitchin, J.G. Chen, S. Pandelov, U. Stimming, Trends in the exchange current for hydrogen evolution, J. Electrochem. Soc. 152 (3) (2005) J23–J26.

[14] T.F. Jaramillo, K.P. Jørgensen, J. Bonde, J.H. Nielsen, S. Horch, I. Chorkendorff, Identification of active edge sites for electrochemical H2 evolution from MoS2 nanocatalysts, Science (1979) 317 (5834) (2007) 100–102, https://doi.org/10.1126/science.1141483.

[15] J. Kibsgaard, Z. Chen, B.N. Reinecke, T.F. Jaramillo, Engineering the surface structure of mos2 to preferentially expose active edge sites for electrocatalysis, Nat. Mater. 11 (11) (2012) 963–969.

[16] H. Tang, K. Dou, C.-C. Kaun, Q. Kuang, S. Yang, MoSe2 nanosheets and their graphene hybrids: synthesis, characterization and hydrogen evolution reaction studies, J. Mater. Chem. A Mater. 2 (2) (2014) 360–364, https://doi.org/10.1039/C3TA13584E.

[17] J.C. McGlynn, T. Dankwort, L. Kienle, N.A.G. Bandeira, J.P. Fraser, E.K. Gibson, I. Cascallana-Matías, K. Kamarás, M.D. Symes, H.N. Miras, A.Y. Ganin, The rapid electrochemical activation of MoTe2 for the hydrogen evolution reaction, Nat. Commun. 10 (1) (2019) 1–9, https://doi.org/10.1038/s41467-019-12831-0.

[18] D. Lu, X. Ren, L. Ren, W. Xue, S. Liu, Y. Liu, Q. Chen, X. Qi, J. Zhong, Direct vapor deposition growth of 1T′ MoTe2 on carbon cloth for electrocatalytic hydrogen evolution, ACS Appl. Energy Mater. 3 (4) (2020) 3212–3219, https://doi.org/10.1021/acsaem.9b01589.

[19] J.B. Mc Manus, G. Cunningham, N. McEvoy, C.P. Cullen, F. Gity, M. Schmidt, D. McAteer, D. Mullarkey, I. Shvets, P.K. Hurley, T. Hallam, G.S. Duesberg, Growth of 1T′ $MoTe_2$ by thermally assisted conversion of electrodeposited tellurium films, ACS Appl. Energy Mater. 2 (1) (2019) 521–530, https://doi.org/10.1021/acsaem.8b01540.

[20] H. Li, X. Jia, Q. Zhang, X. Wang, Metallic transition-metal dichalcogenide nanocatalysts for energy conversion, Chem 4 (7) (2018) 1510–1537, https://doi.org/10.1016/j.chempr.2018.03.012.

[21] E. Dashjav, A. Szczepenowska, H. Kleinke, Optimization of the thermopower of the antimonide Mo3Sb7 by a partial SB/Te substitution, J. Mater. Chem. 12 (2) (2002) 345–349, https://doi.org/10.1039/b107468g.

[22] H. Zhang, J. He, B. Zhang, Z. Su, T.M. Tritt, N. Soheilnia, H. Kleinke, Thermoelectric properties of Mo 3Sb 5.4Te 1.6 and Ni 0.06Mo 3Sb 5.4Te 1.6, J. Electron. Mater. 36 (7) (2007) 727–731, https://doi.org/10.1007/s11664-006-0085-1.

[23] L. Baggetto, E. Allcorn, R.R. Unocic, A. Manthiram, G.M. Veith, Mo3Sb7 as a very fast anode material for lithium-ion and sodium-ion batteries, J. Mater. Chem. A Mater. 1 (37) (2013) 11163–11169, https://doi.org/10.1039/C3TA12040F.

[24] X. Shi, Y. Pei, G.J. Snyder, L. Chen, Optimized thermoelectric properties of Mo3Sb7−xTex with significant phonon scattering by electrons, Energy Environ. Sci. 4 (10) (2011) 4086–4095, https://doi.org/10.1039/C1EE01406D.

[25] P. Jensen, A. Kjekshus, The crystal structure of Mo3Sb7, Acta Chem. Scand. 20 (1966).

[26] H. Okabe, S. Yano, T. Muranaka, J. Akimitsu, Magnetic and structural phase transitions in Mo3Sb7, J. Phys. Conf. Ser. 150 (5) (2009) 52196, https://doi.org/10.1088/1742-6596/150/5/052196.

[27] C. Candolfi, B. Lenoir, A. Dauscher, J. Tobola, S.J. Clarke, R.I. Smith, Neutron diffraction and ab initio studies of Te site preference in Mo3Sb7−xTex, Chem. Mater. 20 (20) (2008) 6556–6561, https://doi.org/10.1021/cm801560n.

[28] H. Xu, K.M. Kleinke, T. Holgate, H. Zhang, Z. Su, T.M. Tritt, H. Kleinke, Thermoelectric performance of NiyMo3Sb7−xTex ($Y \leq 0.1$, $1.5 \leq x \leq 1.7$), J. Appl. Phys. 105 (5) (2009) 53703, https://doi.org/10.1063/1.3086641.

[29] H. Wan, X. Liu, H. Wang, R. Ma, T. Sasaki, Recent advances in developing high-performance nanostructured electrocatalysts based on 3d transition metal elements, Nanoscale Horiz. 4 (4) (2019) 789–808, https://doi.org/10.1039/C8NH00461G.

[30] Sung Wng Kim, Young Hee Lee, Young-Woo Son, Heejun Jinbong Seok, Jun-Ho Lee, Suyeon Cho, Byungdo Ji, Hyo Won Kim, Min Kwon, Dohyun Kim, Young-Min Kim, Sang Ho Oh, Y. Active hydrogen evolution through lattice distortion in metallic MoTe 2. *2d Mater* **2017**, *4* (2), 25061.

[31] J.C. McGlynn, I. Cascallana-Matías, J.P. Fraser, I. Roger, J. McAllister, H.N. Miras, M.D. Symes, A.Y. Ganin, Molybdenum ditelluride rendered into an efficient and stable electrocatalyst for the hydrogen evolution reaction by polymorphic control, Energy Technology 6 (2) (2018) 345–350, https://doi.org/10.1002/ente.201700489.

[32] X. Liu, H. Jang, P. Li, J. Wang, Q. Qin, M.G. Kim, G. Li, J. Cho, Antimony-based composites loaded on phosphorus-doped carbon for boosting faradaic efficiency of the electrochemical nitrogen reduction reaction, Angew. Chem. Int. Ed. 58 (38) (2019) 13329–13334, https://doi.org/10.1002/anie.201906521.

[33] H. Nan, Y. Liu, Q. Li, P. Shen, K. Chu, A janus antimony sulfide catalyst for highly selective N2 electroreduction, Chem. Commun. 56 (71) (2020) 10345–10348, https://doi.org/10.1039/D0CC04764C.

[34] S. Ibraheem, X. Li, S.S.A. Shah, T. Najam, G. Yasin, R. Iqbal, S. Hussain, W. Ding, F. Shahzad, Tellurium triggered formation of Te/Fe-NiOOH nanocubes as an efficient bifunctional electrocatalyst for overall water splitting, ACS Appl. Mater. Interfaces 13 (9) (2021) 10972–10978, https://doi.org/10.1021/acsami.0c22573.

[35] C. Tsai, K. Chan, J.K. Nørskov, F. Abild-Pedersen, Theoretical insights into the hydrogen evolution activity of layered transition metal dichalcogenides, Surf. Sci. 640 (2015) 133–140, https://doi.org/10.1016/j.susc.2015.01.019.

[36] E.J. Popczun, J.R. McKone, C.G. Read, A.J. Biacchi, A.M. Wiltrout, N.S. Lewis, R. E. Schaak, Nanostructured nickel phosphide as an electrocatalyst for the hydrogen evolution reaction, J. Am. Chem. Soc. 135 (25) (2013) 9267–9270, https://doi.org/10.1021/ja403440e.

[37] E. Kovalska, P.K. Roy, N. Antonatos, V. Mazanek, M. Vesely, B. Wu, Z. Sofer, Photocatalytic activity of twist-angle stacked 2D TaS2, npj 2D Mater. Appl. 5 (1) (2021) 68, https://doi.org/10.1038/s41699-021-00247-8.

[38] H. Kwon, D. Bae, H. Jun, B. Ji, D. Won, J.-H. Lee, Y.-W. Son, H. Yang, S. Cho, Basal-plane catalytic activity of layered metallic transition metal ditellurides for the hydrogen evolution reaction, Appl. Sci. 10 (9) (2020), https://doi.org/10.3390/app10093087.

[39] J. Yang, A.R. Mohmad, Y. Wang, R. Fullon, X. Song, F. Zhao, I. Bozkurt, M. Augustin, E.J.G. Santos, H.S. Shin, W. Zhang, D. Voiry, H.Y. Jeong, M. Chhowalla, Ultrahigh-current-density niobium disulfide catalysts for hydrogen evolution, Nat. Mater. 18 (12) (2019) 1309–1314, https://doi.org/10.1038/s41563-019-0463-8.